UDC: 504.3.054: 544.723.23: 544.772: 547-302

M. S. Bazylevska*, V. I. Bogillo

Institute of Geological Sciences, National Academy of Sciences of Ukraine,
55B O. Gonchara Str., Kyiv, 01054, Ukraine

* Corresponding author: bazilevskaya1955@gmail.com

ADSORPTION PROPERTIES OF THE FUMED INDIVIDUAL AND MIXED SI, TI AND AL OXIDES AS PROXIES FOR THE ANTARCTIC ATMOSPHERIC MINERAL AEROSOLS

ABSTRACT. **The aim of the study** is to determine the effects of structure and content of X, C_X in the oxides X/SiO_2 ($X = Al_2O_3$, TiO_2, Al_2O_3/TiO_2) on the surface characteristics. The low-temperature nitrogen adsorption isotherms on the surface of 12 individual and mixed fumed oxides of Si, Ti and Al, as proxies for the Antarctic atmospheric mineral aerosols, were measured by volumetric **method**. The specific surface areas of the oxides, S_{BET} were calculated by using the Brunauer–Emmett–Teller (BET) theory. The dependence between C_X and S_{BET} is not obeyed for the mixed oxides, which can be caused by effects of the reaction temperature of MCl_n (M = Si, Ti and Al) hydrolysis in the oxygen/hydrogen flame and by different concentration ratios of O_2, H_2 and MCl_n on the structural characteristics of the primary particles and their aggregates. The N_2 adsorption energy distributions of the oxides surface were calculated by the regularization procedure. It was demonstrated that the surfaces are characterized by high energetic heterogeneity. **Result.** The Zero-Adsorption Isotherm (ZAI) approach was applied to describe the N_2 adsorption in the whole range of its pressures. The ZAI derived in approximation of adsorbed vapor as a set of molecular clusters. The specific surface areas for the oxides, A_s, maximal numbers of the molecules in the adsorbed clusters, thicknesses of the adsorbed liquid film and the free surface energies of the oxides in the absence of adsorption, γ^{S0}, were calculated using the ZAI equations. The A_s correlates well with S_{BET} and it measures 77.5% of the S_{BET}. The γ^{S0} increases as the N_2 average adsorption energy grows. The dependence between γ^{S0} and C_X (taking into account γ^{S0} for X) is not obeyed for the mixed oxides. The γ^{S0} for SiO_2, Al_2O_3 and TiO_2 rises as the permittivity and the index of refraction increase. The γ^{S0} is within the range of dispersive components of free surface energy, which is determined by other experimental methods and calculated using the Lifshitz' theory. The obtained parameters allow estimate the activity of the oxide surface with respect to trace gases in the Antarctic atmosphere that is necessary for calculating their partition coefficients between particles and the atmosphere and the kinetics of their removal.

Keywords: mineral aerosols, Antarctic atmosphere, fumed individual and mixed Si, Ti and Al oxides, nitrogen adsorption.

INTRODUCTION

Atmospheric aerosols play a major role in Earth's current climate due to their impact on the global radiation balance (Seinfeld and Pandis, 2006). Aerosols also lead to formation of cloud droplets and ice crystals by serving as cloud condensation nuclei (CCN) and ice nuclei particles (INP). Aerosols affect the lifetime of clouds, size distributions of cloud droplets, glaciation rates and the distribution of water mass in different atmospheric layers. Unfortunately, aerosols are still the least understood and constrained aspects of the climate system. The uncertainty of aerosols' climate impacts arise from the fact that how an aerosol affects the radiative balance is a function of both an aerosol's chemical composition and physical properties (e.g. size, shape). Both chemical and physical properties of aerosols are functions of emission sources, atmospheric processing pathways, and lifetime in the atmosphere.

Cite: Bazylevska M. S., BogilloV. I. Adsorption properties of the fumed individual and mixed Si, Ti and Al oxides as proxies for the Antarctic atmospheric mineral aerosols. *Ukrainian Antarctic Journal*, 2019. № 1(18), 3–17.

The atmosphere above Antarctica constitutes the cleanest part of the Earth's troposphere which allows here to study the composition and temporal change of the background atmosphere without any direct impact of civilization. Furthermore, with the exception of very few rocky terrains, the Antarctic continent is largely free of aerosol sources, so that the main part of the particles must be advected by long-range transport to Antarctica or has its source region in the surrounding Southern Ocean. Due to this unique position, Antarctica is an outstanding place to document long-term changes of the composition of our atmosphere in the industrial period. The Antarctic climate system can be linked with aerosol particles by complex feedback processes that involve aerosol-cloud interactions. In addition, because there are less anthropogenic emission sources in Antarctica, it is a suitable place to study the formation and growth processes of the natural aerosol particles. Mineral dust is extremely important in the nucleation processes, as sites for heterogeneous chemistry. Particles are formed from a large numbers of minerals, e.g. alumina, silica and iron oxides, coated with sulfates, nitrates and organic species as small particles in the atmosphere. Mineral dust always acts like solid core for trace gases condensation on their surface.

Another important aspect of studying mineral aerosols in Antarctica is the need to interpret records of particulates observed in firn and ice cores. Mineral dust is one of the more studied paleoclimatic and paleo-environmental proxies among those that can be recovered from the ice cores. Dust particles arrive in the remote polar area after long-range transport from deserted and semi-deserted continental areas located at lower latitudes. Many characters of dust in the ice are measured, because of their potential to provide paleo-climatic information on the location and aridity at the dust sources, the scavenging and transport processes, and the atmospheric pathways.

Although global dust sources are absent, Antarctica is the largest polar desert in the world, where approximately 2% of its surface area is ice-free and contains active High Latitude Dust sources (HLD, Bullard et al., 2016). The best-known local dust sources are located in West Antarctica, with the McMurdo Dry Valleys being the largest ice free area (approximately 4,800 km^2) with frequent dust suspension (Lancaster, 2002; Ayling and McGowan, 2006; Atkins and Dunbar, 2009; Bullard et al., 2016). As it follows from dust samples collected in snow pits on Berkner Island, the dust sources are located also in the ice-free areas of East Antarctica (Bory et al. 2010). Coastal ice-free areas have also been identified as active dust sources around the Maitri Station, Larsemann Hills, and Neumayer Station in East Antarctica (Weller et al., 2008; Chaubey et al., 2011; Budhavant et al., 2015), as well as in the Antarctic Peninsula region (Artaxo and Rabello, 1992; Kavan et al., 2017; Asmi et al., 2018). Alternately, the mineral particles can be re-suspended from the surface of ablating glaciers (Atkins and Dunbar, 2009). Long-range transport of dust from other HLD sources, such as South America (Patagonia), New Zealand, and deserts in Australia and Africa, contribute to the dust depositions in Antarctica (Ne and Bertler, 2015; Bullard et al., 2016; Asmi et al., 2018). The main non-Antarctic dust source for the Antarctic Peninsula region is in Patagonia (Bullard et al., 2016). Patagonian dust was found in ice cores and snow samples in the Antarctic Peninsula and in East Antarctica (Basile et al., 1997; Pereira et al., 2004; McConnell et al., 2007; Bory et al., 2010; Delmonte et al., 2017).

The dust deposition rates of > 100 g m^{-2} year^{-1} were reported from Patagonia (Bullard, 2016). The rates measured in McMurdo Dry Valleys (< 8 g m^{-2} year^{-1}) are lower than other HLD sources (Lancaster, 2002). Nevertheless, the dust fluxes of 7.8—24.5 g m^{-2} year^{-1} (Atkins and Dunbar, 2009) and 0.2—55 g m^{-2} year^{-1} (Chewings et al. 2014) are reported in this source. The mass concentrations of PM_{10} (particles with a diameter of < 10 μm) and $PM_{2.5}$ (with a diameter of < 2.5 μm) in boundary atmospheric layer were 5.1 and 4.3 mg m^{-3}, respectively in the Larsemann Hills during summer (Budhavant et al., 2015), and 8.3 and 6.03 mg m^{-3} at the Maitri station (Chaubey et al., 2011). PM_{10} concentrations from McMurdo station during two summers in 1995—1997 were 3.4 and 4.1 mg m^{-3} on average (Mazzera et al., 2001). Mean PM_{10} and $PM_{2.5}$ concentrations of 4.4 mg m^{-3} and 2.4 mg m^{-3}, respectively were measured in the

Antarctic Peninsula during the late 1980s (Artaxo and Rabello, 1992). Seasonal variations in aerosol loadings showed increased concentrations in January and a decrease in February and March in Terra Nova Bay, West Antarctica in 2000—2001 (Truzzi et al., 2005). PM_{10} concentrations of 2.1—5 mg m^{-3} on average were reported from the Antarctic Peninsula, with higher concentration in summer (October to March) in 2013—2015 (Asmi et al., 2018). The concentrations of the particles nearly doubled in summer when winds were high (Asmi et al. 2018).

Because mineral dust may undergo processing as it is transported in the atmosphere, its impact on global processes may change over the course of its "life story". Therefore, knowledge of its physicochemical properties, especially its adsorption characteristics, is very important for predicting its effects in atmospheric chemistry and biogeochemical cycles in Antarctica. Most of the experiments on the interaction of trace gases with mineral dust were performed with oxides such as SiO_2, Al_2O_3, and CaO (Pokrovskiy et al., 1999; Al-Abadleh and Grassian, 2003).

The surface of mineral dust particles acts as a sink for many gases, such as sulfur dioxide (SO_2), with the formation of sulfite ion (SO_3^{2-}) associated with it, which is oxidized to sulfate ion (SO_4^{2-}) in the presence of ozone or other oxidizing agents. However, an evidence has recently been obtained of an alternative way of generating these ions for a series of reactions: in the presence of water vapor, titanium oxides, iron or mineral dust containing these oxides, exposure to the UV part of solar radiation produces gaseous sulfuric acid (H_2SO_4), which then reacts with the surface of the particles (Dupart et al, 2012). Metal oxides in mineral dust act as atmospheric photocatalysts, promoting the formation of gaseous OH radicals, which initiate the conversion of SO_2 to H_2SO_4 in the vicinity of the particle. At a low concentration of dust in the atmosphere characteristic over Antarctica, this process can lead to the nucleation phenomena and the formation of the CCN.

In the present work, highly dispersed fumed silica, alumina, titania, and mixed X/SiO_2 oxides (X = = Al_2O_3, TiO_2 and Al_2O_3/TiO_2) are used as proxies of mineral aerosols. These oxides produced by condensation processes are often of more theoretical interest because it is easier to control their nucleation and growth rate, particle size and size distribution, and rate of disappearance. They can therefore be used more readily to study the various theories of aerosol formation and destruction. The choice of oxides SiO_2 and Al_2O_3 is due to their dominance in the earth's crust and in the composition of the mineral dust as ice nucleating particles, while TiO_2 has semiconductor properties and can serve as a natural photocatalyst for the formation of H_2SO_4, which is the main component of CCN that have a significant impact on the Antarctic climate. Natural analogues of these oxides can be mineral particles formed during volcanic eruptions, for example, Mt. Erebus in Antarctica, as a result of high-temperature hydrolysis of metal halides, $MHal_n$ (M = Si, Al, Ti; Hal = Cl, Br, I) in presence of water vapor. Nitrogen was used as an adsorbed substance. The main goal of the work was to determine the influence of the oxides composition on the adsorption characteristics of their surface.

MATERIALS AND METHODS

Highly dispersed fumed individual silica, alumina, titania and mixed oxides X/SiO_2 (X = Al_2O_3, TiO_2, Al_2O_3/TiO_2) (synthesized at the experimental plant of the Institute of Surface Chemistry of the National Academy of Sciences of Ukraine, Kalush, Ukraine) were studied at various concentrations (C_X) phase X oxide (Table 1). Titania, titania/silica and alumina/titania/silica contain a mixture of anatase (particle shell, main part) and rutile (core of particles). Alumina includes ≈ 20% (by weight) of the crystalline γ-phase and ≈ 80% of the amorphous phase, whereas in alumina/silica and alumina/titania/silica it is completely amorphous. Silica is completely amorphous in all fumed oxides. Alumina/titania/silica includes ≈ 22% Al_2O_3, ≈ 28% SiO_2 and ≈ 50% TiO_2 (a mixture of 88% anatase and 12% rutile). The phase composition and other properties of these mixed oxides are reported in (Gun'ko et al. 2007).

The nitrogen adsorption/desorption isotherms on the oxide surfaces were measured at 77.35 K and relative pressure $x = P/P_S$ (P and P_S are the equilibrium

vapor pressure of nitrogen and its saturated vapor pressure, respectively) in the range from $\approx 5 \times 10^{-7}$ to ≈ 0.99 by using an ASAP 2010 V-3.00 volumetric multigas sorption analyzer (Micromeritics, Norcross, GA). Before measurements, the samples were subjected to treating in vacuum at 393 K for 6 hours to remove physically adsorbed water and other volatile impurities from the surface of the oxides. The total pore volume was estimated by converting the volume adsorbed at the relative pressure of 0.985 to the volume of liquid nitrogen.

Methods for the calculation of adsorption parameters

BET theory

The specific surface area of the samples was calculated in accordance with standard Brunauer – Emmett – Teller (BET) procedure based on adsorption data in the $x = P/P_S$ range from 0.06 to 0.25 (Brunauer et al., 1938; Gregg et al, 1982)

$$\frac{a}{a_m} = \frac{Cx}{(1-x)[1+(C-1)x]} \quad (1)$$

$$S_{BET} = a_m \sigma_m N_A \quad (2)$$

$$C \approx \exp\left(\frac{\Delta Q_A - \Delta Q_V}{RT}\right), \quad (3)$$

where a is the number of moles of adsorbed substance per unit weight of adsorbent (mol g^{-1}), a_m is the capacity of the monolayer of adsorbed substance per unit weight of adsorbent, σ_m is the average area occupied by the adsorbed molecule in the monolayer (for N_2 it is assumed to be 16.2 Å^2), N_A is the Avogadro number, ΔQ_A is the average differential heat of adsorption, ΔQ_V is the heat of vaporization of the adsorbed substance, R is the universal gas constant, T is the adsorption temperature in K.

Regularization procedure

The nitrogen adsorption in the monolayer taking into account the energetic heterogeneity of the oxide surface was studied using the modified regularization procedure proposed in (Pyziy et al., 1997; Bogillo and Shkilev, 1999). Using the capacities of the monolayer obtained by the BET method, a_m, for those values of a for which $a_m \geq a$, we can determine the overall surface coverage with adsorbed substance within the monolayer, $\Theta(P,T) = a/a_m$. Adsorption within these limits is generally described by the Fredholm integral equation of the first kind

$$\Theta(P,T) = \int_{E_{A(\min)}}^{E_{A(\max)}} \theta(P, T, E_A)\, \rho(E_A)\, dE_A, \quad (4)$$

where $\theta(P, T, E_A)$ is the coverage of the local surface area with the adsorption energy E_A, $\rho(E_A)$ is the normalized differential surface distribution on E_A, $E_{A(\min)}$ and $E_{A(\max)}$ are the lower and upper limits of this distribution.

In the simplest case, the local coverage, $\theta(P, T, E_A)$, is described by the Langmuir isotherm:

$$\theta(P, T, E_A) = \frac{P \times K_{L,0}^{-1} \exp(E_A/RT)}{1 + P \times K_{L,0}^{-1} \exp(E_A/RT)}, \quad (5)$$

where $K_{L,0}$ is a preexponential factor depending on the rotational, vibrational, and translational degrees of freedom of a polyatomic molecule adsorbed on the surface and in the gas phase. This value can be approximately estimated using the ratio (Bogillo et al., 1998)

$$K_{L,0} \approx P_s \exp(\Delta Q_V / RT). \quad (6)$$

One of the important problems in describing adsorption equilibria on a heterogeneous surface remains the choice of the minimum information necessary for a stable calculation of the distribution $\rho(E_A)$. The main idea of the numerical regularization is to replace the ill-posed problem of minimizing the selected function by a well-posed problem which smoothes the calculated distribution and distorts the origin problem insignificantly. Thus, the solution of equation (4) is replaced by minimizing the functional:

$$\Phi[\rho(E_A)] = \left\{ \int_{E_{A(\min)}}^{E_{A(\max)}} \theta(P, T, E_A)\, \rho(E_A) dE_A - \Theta(P,T) \right\}^2 + \alpha \int_{E_{A(\min)}}^{E_{A(\max)}} \rho^2(E_A) dE_A. \quad (7)$$

where α ($1 \geq \alpha > 0$) is the regularization parameter depending on the relative errors in determining the adsorption isotherm.

To obtain the optimal α, we proposed a two-step procedure. First, the functional $\Phi[\rho(E_A)]$ is minimized at $\alpha = 0$. Thus, this minimum can serve as an measure of the accuracy of experimental data for m points on the adsorption isotherm:

$$\xi = \min\left[\frac{1}{m}\sum_{j=1}^{m}\left(\Theta(P,T) - \theta(P,T,E_A)\rho^0(E_A)\right)^2\right]^{1/2}.$$

In the second step, the value of α is calculated at which the distribution $\rho^1(E_A)$, which minimizes the functional $\Phi[\rho(E_A)]$, satisfies the following condition:

$$\eta \times \xi = \min\left[\frac{1}{m}\sum_{j=1}^{m}(\theta(p, T, E_A)\rho^0(E_A) - \theta(p, T, E_A)\rho^1(E_A))^2\right]^{1/2}. \quad (9)$$

A feature of this modified method is the possibility of improving the solution by varying the free parameter η. The calculations showed that none of the methods for estimating α proposed in the literature leads to stable solutions of equation (4) in the absence of η. The distributions $\rho(E_A)$ were calculated on the basis of part of the nitrogen adsorption isotherms corresponding to the monolayer surface coverage.

ZAI theory

A new isotherm, so-called Zeta Adsorption Isotherm (ZAI) was recently derived to describe accurately the adsorption in the full range of P up to P_S (Zandavi et al., 2014). This isotherm is obtained in the approximation of adsorbed vapor as a set of molecular clusters, of which at least one is adsorbed by one of the M adsorption sites. Each adsorbed cluster is approximated as a quantum-mechanical harmonic oscillator with a binding energy that depends on the number of molecules in the cluster. The maximum number of molecules which cluster can consist of is ζ_m. Using the canonical ensemble, the dependence of the amount of adsorbed matter on the solid/vapor interface per unit surface on the vapor pressure ratio is described as

$$a = \frac{Mc_Z\alpha_Z x\,[1-(1+\varsigma_m)(\alpha_Z x)^{\varsigma_m} + \varsigma_m(\alpha_Z x)^{1+\varsigma_m}]}{(1-\alpha_Z x)[1+(c_Z-1)\alpha_Z x - c_Z(\alpha_Z x)^{1+\varsigma_m}]}. \quad (10)$$

Parameters c_Z and α_Z are related to distribution of the clusters with different number of molecules and to the chemical potential of the adsorbed liquid at standard pressure, respectively.

In ZAI, the number of adsorption sites per unit of mass of a solid, M_g is related to the specific surface area, A_s, as

$$M_g = A_s M. \quad (11)$$

In the derivation of ZAI, it is assumed that one molecular cluster occupies one adsorption site. The average cross-sectional area of the adsorption site or the molecular cluster of a given vapor (I) is denoted as $\sigma(I)$. Then the specific adsorption surface area of the solid, A_s is given as

$$\sigma(I)\, M_g(I) = A_s. \quad (12)$$

When the specific volume of the adsorbed liquid film is equal to that for a pure liquid in the volume, v_f, the thickness of the adsorbed liquid film, τ_{af}, is defined as

$$\tau_{af} = \frac{M_g \varsigma_m v_f}{A_s}. \quad (13)$$

Equation 10 together with the Gibbs adsorption equation for this surface allows to derive the ratio for surface tension or free surface energy of a solid in the absence of adsorption, γ^{S0} (Ghasemi et al., 2009):

$$\gamma^{S0} = \gamma^{LV} + Mk_B T \ln\left[1 + \frac{c_Z\alpha_Z}{1-\alpha_Z}\right], \quad (14)$$

where γ^{LV} is the surface tension or free surface energy of the adsorbed substance in the liquid/vapor system and k_B is the Boltzmann constant.

Lifshitz theory

The value of γ^{S0}, in the general case, is the sum of the dispersive, γ_S^D and polar, γ_S^p components of the free surface energy:

$$\gamma^{S0} = \gamma_S^D + \gamma_S^p. \quad (15)$$

The dispersive component, γ_S^D is related to the Hamaker constant of the material, A_H (Israelachvili, 1992):

$$A_H = 24\pi D_0^2 \gamma_S^D, \quad (16)$$

where D_0 is the smallest equilibrium distance between two identical materials in a vacuum. Given the Born repulsion, this distance is 1.6 A.

On the other hand, the approximate expression from the Lifshitz' theory for A_H in vacuum or in air can be written as (Dzyaloshinskii et al., 1961):

$$A_H \cong \frac{3}{4} k_B T \left(\frac{\varepsilon_k - 1}{\varepsilon_k + 1}\right)^2 + \frac{3h\nu_c \left(n_0^2 - 1\right)^2}{16\sqrt{2}\left(n_0^2 + 1\right)^{3/2}}, \quad (17)$$

where n_0 is the refractive index, ε_k is the permittivity of the material, ν_c is the main frequency of electron absorption in the UV range ($\nu_c = (3 \div 5) \times 10^{15}$ s^{-1}), and h is the Planck constant ($h = 6.626 \times 10^{-34}$ J s).

RESULTS AND DISCUSSION

Fumed oxides, such as silica, titania, alumina, silica/alumina, titania/silica, alumina/titania/silica are widely used in industry as adsorbents, pigments, catalysts, fillers and additives in polymers. There is a multistage hierarchy of the oxides structure related to the features of their synthesis when using MCl_n (M = = Si, Ti, and Al) in an oxygen/hydrogen flame at $T >$ 1300 K. Variations in the reaction temperature and the ratio between the O_2/H_2 and MCl_n concentrations affect the structural characteristics of the primary particles and the concentration of hydroxyl groups on the surface of the oxides. Nonporous spherical primary particles with a diameter of 5—100 nm, depending on the synthesis conditions and the composition of the oxides, form aggregates with a diameter of 100—500 nm, and then loose agglomerates (>1 μm). These structural levels differ significantly in apparent density, ρ_{ap}. For example, for fumed silica, ρ_{ap} is 1—3% for agglomerates, ~30% for aggregates, and ~100% of the specific density of primary particles (Gun'ko et al.,

Table 1. **The specific adsorption area of the oxides surface, S_{BET}, the C constant of the BET equation, the nitrogen average isosteric adsorption heat, ΔQ_A, the apparent pore volume, v_p, the nitrogen average adsorption energy in the monolayer, $E_{A(av)}$ and its standard deviation, σ_{Ea}**

Sample	Composition	S_{BET}	v_p	C	ΔQ_A	$E_{A(av)}$	σ_{Ea}
		m^2g^{-1}	cm^3g^{-1}		kJ mole^{-1}		
T_{100}	100% TiO_2	60	0.17	98	8.53	7.9	2.9
ST_{29}	SiO_2-29%TiO_2	73	0.16	93	8.49	7.3	4.2
ST_{20}	SiO_2-20%TiO_2	65	0.13	263	9.16	7.6	6.5
ST_{14}	SiO_2-14%TiO_2	217	0.49	117	8.64	6.6	3.1
ST_9	SiO_2-9%TiO_2	198	0.47	116	8.63	7.1	2.2
S_{100}	100%SiO_2	267	0.62	126	8.69	7.1	2.5
$SA_{1..3}$	SiO_2-1.3%Al_2O_3	294	0.68	129	8.70	7.7	1.6
SA_3	SiO_2-3%Al_2O_3	156	0.35	165	8.86	7.6	4.7
SA_{23}	SiO_2-23%Al_2O_3	311	0.74	106	8.58	7.4	1.6
SA_{30}	SiO_2-30%Al_2O_3	239	0.57	106	8.58	7.5	1.8
A_{100}	100%Al_2O_3	159	0.42	133	8.72	7.3	1.5
SAT	SiO_2-22%Al_2O_3-50%TiO_2	32	0.08	97	8.52	6.9	8.3

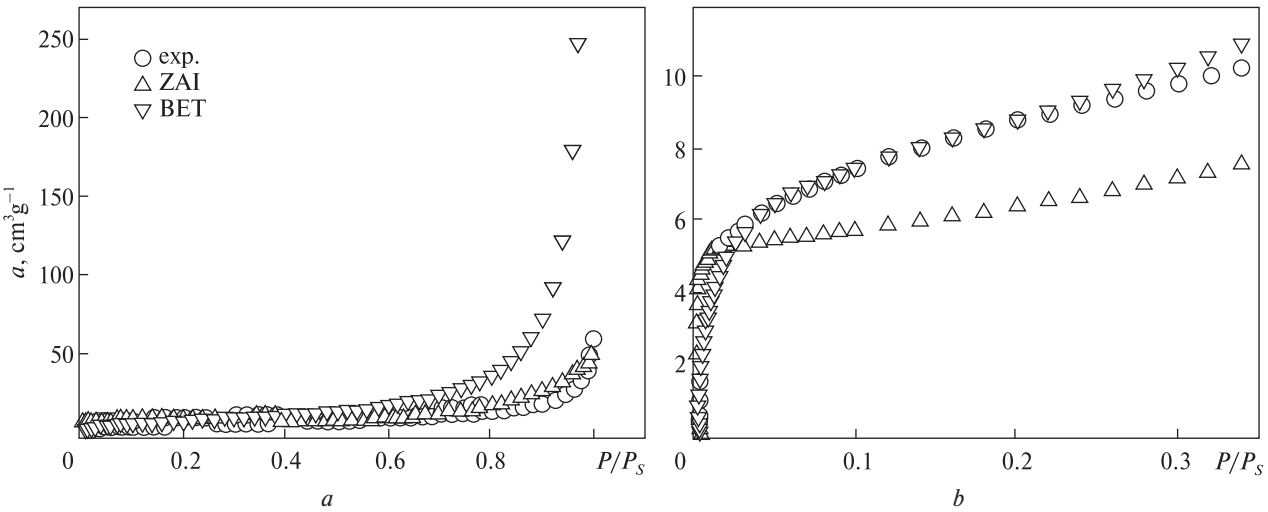

Fig. 1. Experimental and calculated according to the theories of ZAI and BET nitrogen adsorption isotherms on the surface of alumina/titania/silica (SAT) at 77.35 K in the P/P_S range from 0 to 1.0 (*a*) and up to 0.35 (*b*)

2007). The smaller these particles, the stronger they are bound in the aggregates and the narrower is the particle size distribution.

Roughness and amorphisms of the particle surface, variations in the types and concentration of hydroxyl groups on the surface can be the main reasons for the structural and energetic heterogeneity of the oxides surface with respect to various adsorbates. Since some phases in mixed oxides are amorphous (SiO_2, Al_2O_3), while others, for example, TiO_2, can be crystalline, their surface heterogeneity can increase. The interfaces between the amorphous and crystalline phases in such oxides include strained bonds, incompletely coordinated metal atoms (Lewis acid centers), single and bridged hydroxyl groups (Bronsted acid centers), strongly bonded water molecules, and other adsorption centers that cause high surface heterogeneity.

One of the main characteristics of the adsorption capacity of materials is the specific adsorption surface area, S_{BET}. The higher it is, the greater the substance amount is held by a unit weight of the adsorbent, i.e., the more efficient the adsorption. These S_{BET} for the studied oxides are given in Table 1. It also presents the pore volumes of materials, v_p, corresponding to the effective volume, since nitrogen adsorption occurs not only in the internal free volume of the aggregates, but also in the free volume of agglomerates, that is, on the outer surface of the aggregates.

Fig. 1 shows the experimental isotherm of nitrogen adsorption on the surface of mixed SAT oxide (Table 1) in the P/P_S range from 0 to 1.0 (*a*) and up to 0.35 (*b*). Its shape corresponds to the type II adsorption isotherm according to the Brunauer classification (Gregg et al., 1982), which is characteristic of vapor adsorption on the surface of non-porous materials. The absence of a plateau on the adsorption isotherms observed at $P/P_S > 0.9$ (Fig. 1, *a*) and the lack of hysteresis, i. e. coincidence of the adsorption and desorption isotherms, testifies that mesopores contribution in the total pore volume of the studied materials is negligible.

Fumed TiO_2 includes primary crystalline particles of anatase (70÷85%) and rutile (15÷30%), while fumed $Al_2O_3 \approx 20\%$ of its crystalline γ-form. Fumed SiO_2 is completely amorphous. Obviously, the observed decrease in S_{BET} during the transition from silica to titania/silica and titania, as well as close S_{BET} values for silica, silica/alumina and alumina are due to the contribution of crystalline forms of TiO_2 and Al_2O_3 to S_{BET} for mixed oxides. Low v_p indicate the condensation of adsorbed nitrogen in the secondary pores formed due to the interparticle space of the aggregates upon contact of the primary non-porous oxide particles.

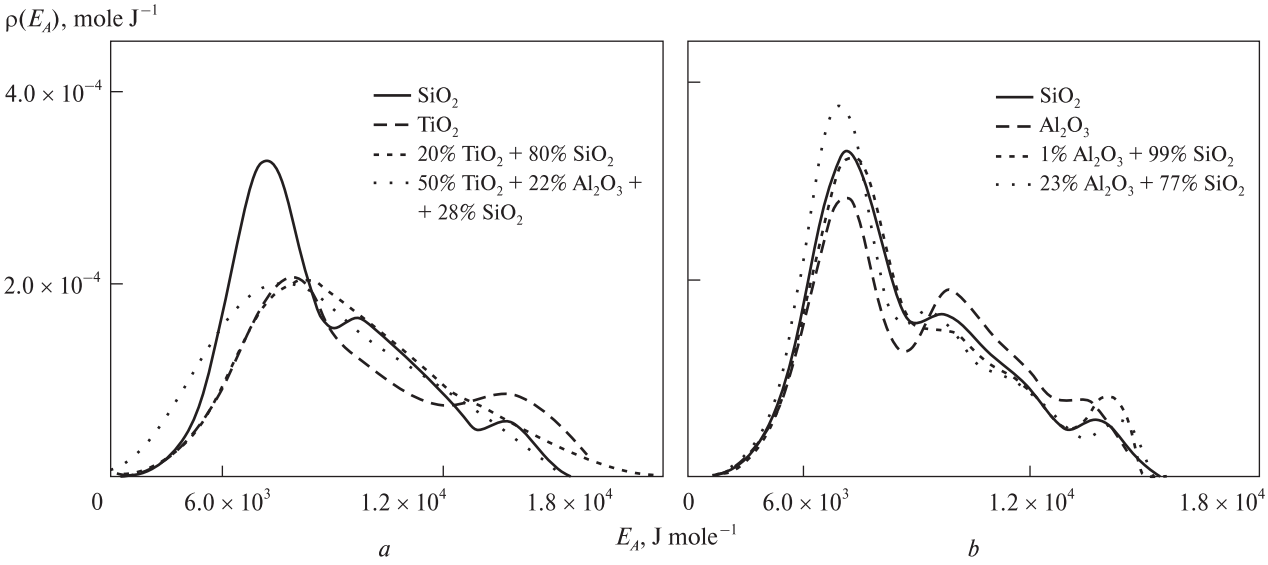

Fig. 2. Distributions of surface of SiO_2, TiO_2, TiO_2/SiO_2, $TiO_2/Al_2O_3/SiO_2$ (a) and SiO_2, Al_2O_3, Al_2O_3/SiO_2 (b) on the N_2 adsorption energy

The average differential heats of nitrogen adsorption calculated on the basis of the *C* constant of the BET equation are given in Table 1. All of them are in a rather narrow range (8.52÷9.16 kJ mol^{-1}), but exceed the heat of vaporization of nitrogen (5.58 kJ mol^{-1}), which is usually equated to the non-specific contribution (dispersion interaction) to the adsorption energy. Such a difference may indicate a significant contribution of the specific (quadrupole – dipole and/or quadrupole – ion) interaction of a quadrupole nitrogen molecule with polar single or bridging OH– surface groups or with coordination-unsaturated metal ions at the oxide phase boundary.

Some distributions of the oxides surface on the N_2 adsorption energy in the monolayer range, which computed by using the regularization procedure, are shown in Fig. 2, *a, b*.

It is seen that the oxides surface is characterized by a high degree of heterogeneity with respect to N_2 adsorption, which manifests itself in the presence of several peaks in the distribution curves and their considerable width. Since the distributions allow only a qualitative comparison of them for the surface of various oxides, we approximated them with a Gaussian distribution. The average N_2 adsorption energies and their standard deviations are given in Table. 1. Note that ΔQ_V for N_2, which characterizes the ability of the dispersion interaction of N_2 with surface sites, is 5.4 kJ mol^{-1}. The upper limits of the distributions significantly exceed this value, which may be due to the contribution of the electrostatic interaction of the quadrupole of N_2 molecule with OH group dipoles and ions of the oxide surface sites. The highest E_A at $\Theta(p.T) \to 0$ (Fig. 2, *a*) and $E_{A(av)} + \sigma_{Ea}$ (Table 1) are typical for TiO_2, ST_{29}, and SAT, in which the content of crystalline phases is maximum.

As follows from Fig. 1, the BET isotherm is close to the experimental one at $P/P_S < 0.3$, but deviates significantly from it at large P/P_S. It is well known that the BET isotherm describes adsorption on the surface of non-porous materials only in a limited pressure range corresponding to the filling of the monolayer (Gregg et al., 1982). At $P \to P_S$, the BET equation predicts infinite adsorption and negative adsorption at $P > P_S$. Other adsorption isotherms (Frenkel – Halsey – Hill or Aranovich – Donahue) more accurately describe adsorption at high *P*, but they also predict infinite adsorption at $P \approx P_S$. Then the Zeta Adsorption Isotherm (ZAI) used here to describe accurately the adsorption in the full range of *P* up to P_S. Table 2 shows the specific surface areas of oxides, A_s, their monolayer capacitances, M_V and M_g,

Table 2. **The specific adsorption area of the oxides surface. A_s, the monolayer capacities. M_V and M_g, the α_Z, c_Z and ζ_m parameters of Eq. 10, and the square of the correlation coefficient for the Eq. 10, R^2**

Sample	A_s, $m^2\ g^{-1}$	M_V, $cm^3\ g^{-1}$	$M_g \times 10^6$, mole g^{-1}	α_Z	c_Z	ζ_m	R^2
T_{100}	43	9,98	445	0,916	6137	70	0,955
ST_{29}	60	13,76	614	0,862	1167	72	0,947
ST_{20}	51	11,68	521	0,862	3096	62	0,946
ST_{14}	176	40,36	1801	0,874	1239	58	0,966
ST_9	159	36,43	1625	0,881	1059	54	0,970
S_{100}	204	46,86	2091	0,885	1650	71	0,963
$SA_{1..3}$	225	51,69	2306	0,887	1833	56	0,959
SA_3	116	26,60	1187	0,882	2053	61	0,956
SA_{23}	240	55,17	2461	0,887	1305	72	0,959
SA_{30}	184	42,23	1884	0,886	1205	59	0,962
A_{100}	123	28,13	1255	0,901	3483	59	0,963
SAT	223	5,24	234	0,897	1954	112	0,933

Table 3. **The thickness of adsorbed N_2 film on the oxides surface, τ_{af}, the free surface energy of the oxides in the absence of adsorption, γ^{S0}, this energy, estimated for mixed oxides, $\gamma^{S0}_{(calc)}$, the dispersive component of free surface energy of the oxides determined by immersion calorimetry, $\gamma^{D}_{(exp)}$, by method of inverse gas chromatography at finite concentrations, $\gamma^{D}_{(IGC)}$, and calculated by the Lifshitz' theory, $\gamma^{D}_{(calc)}$, the refractive indices, n_0 and permittivity, ε_k of individual oxides**

Sample	τ_{af}	γ^{S0}	$\gamma^{S0}_{(calc)}$	$^{a}\gamma^{D}_{(expp)}$	$^{b}\gamma^{D}_{(calc)}$	$^{c}\gamma^{D}_{(IGC)}$	n_0	ε_k
	nm	$mJ\ m^{-2}$						
T_{100}	25	81,8		72	79	35,2	2,8	21,3
ST_{29}	26	67,3	74					
ST_{20}	22	73,7	73			44,9		
ST_{14}	21	68,3	73					
ST_9	19	67,7	72					
S_{100}	25	70,9		32	34	28,6	1,5	4,6
$SA_{1..3}$	20	71,7	71					
SA_3	22	72,1	71					
SA_{23}	26	69,5	72					
SA_{30}	21	68,9	73			32,5		
A_{100}	21	76,9		85	80	51,8	1,8	10,4
SAT	40	72,8	78					

[a] from the calorimetric data of the immersion of oxides in n-heptane (Medout-Marere, 2000). [b] based on the Hamaker constants calculated by the Lifshitz theory (Bergstrom, 1997). [c] from data of inverse gas chromatography at finite concentrations (Bogillo et al., 1996).

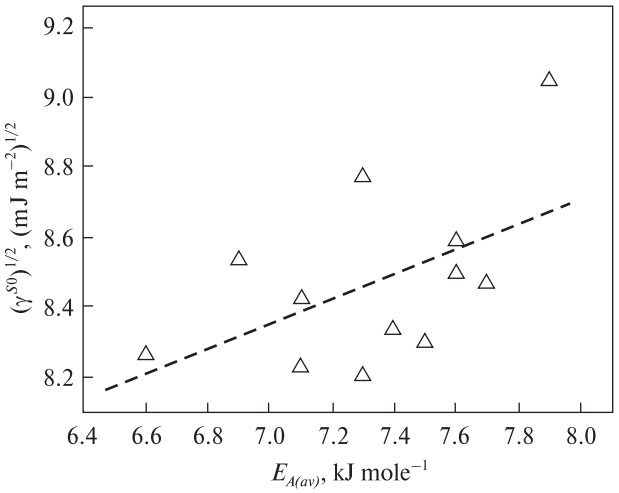

Fig. 3. The surface free energy of the individual and mixed Si, Ti and Al oxides as a function of their average N_2 adsorption energy within the monolayer

the parameters of Eq. 10, and the squares of the correlation coefficients.

As follows from Fig. 1, *a*, the isotherm calculated by the ZAI equation deviates noticeably from experimental one in the range $0 < x < 0.35$, but it is close to the experimental one in the range $0.35 < x < 0.99$, while the isotherm calculated by the BET equation deviates significantly from it and $a \to \infty$ as $x \to 1.0$. Using the $\sigma(N_2) = 16.2$ Å^2 for the surfaces of all oxides, the M equals to $M_g/A_s = 1.0244 \times 10^{-5}$ mole m^{-2}. A comparison of the A_s values with the S_{BET} from Table 1 indicates a close relationship between them: $A_s = (0.775 \pm 0.012) \cdot S_{BET}$; $R^2 = 0.999$. The lower surface areas obtained using ZAI compared to BET may be due to variations in the orientation of nitrogen molecules (e.g., orthogonal) in clusters (ZAI), in contrast to the strictly parallel orientation of molecules in the adsorbed layer, as is assumed in the classical BET theory.

The Table 3 shows the thicknesses of the adsorbed nitrogen film on the oxide surface, the free surface energies of these oxides in the absence of adsorption, these energies estimated for mixed oxides based on γ^{S0} for component *X* in the oxide, $\gamma^{S0}_{(calc)}$, dispersive components of the free surface energy of individual oxides, determined by the calorimetric method, $\gamma^{D}_{(exp)}$ and by the method of inverse gas chromatography at final concentrations, $\gamma^{D}_{(IGC)}$, calculated using Lifshitz' theory, $\gamma^{D}_{(calc)}$, as well as refractive indices, n_0 and permittivity, ε_k of individual oxides. In the calculations for nitrogen at 71.1 K, $\gamma^{LV} = 10.3$ mJ m^{-2} was used (Prausnitz, 1966).

We estimated γ^{S0} for mixed oxides based on these values for individual oxides and the fraction of component *X*. As can be seen from the data in Table 3, for most mixed oxides, the calculated γ^{S0} exceed the experimental ones by 2.5–6.7 mJ m^{-2}. Only for samples ST_{20}, $SA_{1,3}$, and SA_3 there is a slight excess (by 0.7÷1.1 mJ m^{-2}) of experimental values over the calculated ones.

The assumed additivity of γ^{S0} for mixed oxides is valid for an external mixture of oxides forming particles, while for an internal mixture that is inhomogeneous in volume of a particle, it will be violated. Among the studied individual oxides, silica has a minimum γ^{S0} and is part of all mixed oxides. Therefore, we can assume a higher SiO_2 content in the upper shell of mixed oxide particles compared to its bulk content, while Al_2O_3 and crystalline TiO_2 phases form mainly the core of these particles. This assumption is consistent with the conclusions about the particle structure of fumed mixed oxides in (Gun'ko et al., 2007).

Square root of free surface energy of oxides as a function of the average nitrogen adsorption energy within the monolayer is shown in Fig. 3.

An increase in $E_{A(av)}$ leads to an increase in $(\gamma^{S0})^{1/2}$, and a linear relationship is observed between these parameters:

$$\sqrt{\gamma^{S0}} = (0.4 \pm 0.2) E_{A(av)} + (5.9 \pm 1.3); \; R = 0.523.$$

Thus, using Eqs 16 and 17, we can estimate γ_S^D of the material. The values of n_0 and ε_k for individual oxides are given in the Table 3. The calculated $\gamma_{S\,(calc)}^{D}$ values (in mJ m^{-2}) are varied in sequence: TiO_2 (216) > Al_2O_3(70) > SiO_2(33), which qualitatively coincides with the sequence of changes in γ^{S0} of these oxides (TiO_2 (82) > Al_2O_3(77) > SiO_2(71)). Using A_H calculated taking into account various spectral corrections from (Bergstrom, 1997), lower γ_S^D values for TiO_2 (77÷82 mJ m^{-2}) are obtained, which are

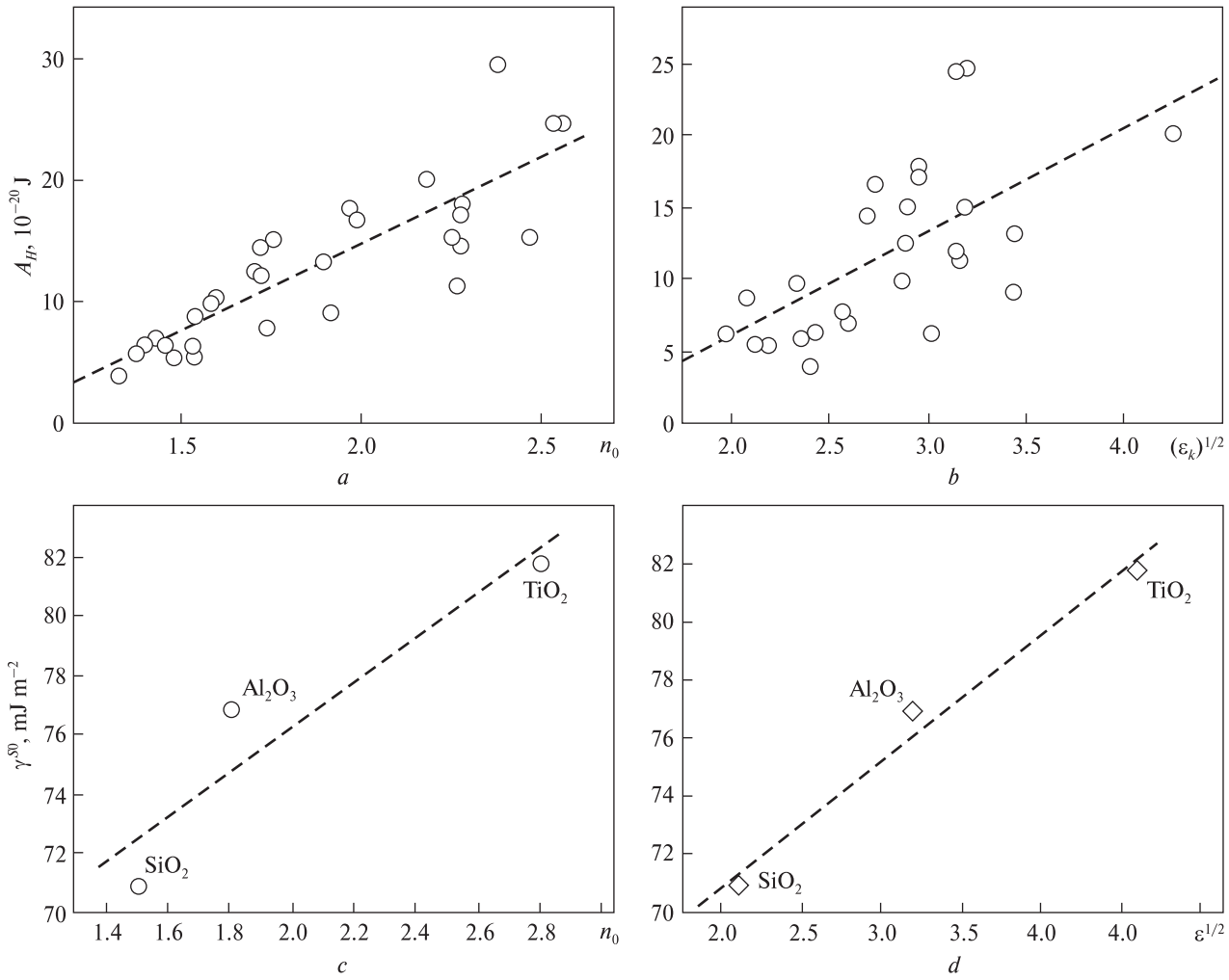

Fig. 4. The dependence of Hamaker constant for inorganic materials (*a, b*) and free surface energy of the metal oxides in the absence of adsorption (*c, d*) on the index of refraction (*a, c*) and on the square root of permittivity of the materials (*b, d*)

close to those found for Al_2O_3 (69÷72 mJ m^{-2}), however for SiO_2 in all cases, the calculation leads to lower γ_S^D (27÷31 mJ m^{-2}).

Plots of A_H for inorganic materials from (Bergstrom, 1997) and γ^{S0} for the oxides on n_0 and $(\varepsilon_k)^{1/2}$ values are shown in Fig. 4. It can be seen that in all cases there is a tendency for A_H and γ^{S0} to increase as the n_0 and $(\varepsilon_k)^{1/2}$ rise. The relations ($A_H \times 10^{-20} = (14.1 \pm 1.6)n_0 - (13.5 \pm 3.1)$, $N = 30$, $R = 0.854$ and $A_H \times 10^{-20} = (7.2 \pm 1.8)\ (\varepsilon_k)^{1/2} - (8.3 \pm 5.1)$, $N = 30$, $R = 0.636$) allow to estimate easy the A_H values of materials.

The γ_S^D value based on A_H determined by calorimetric immersion of metal oxides in n-hexane (Medout-Marere, 2000) is shown in Table 3. It is seen that, in contrast to the calculated γ_S^D and experimental γ^{S0}, the reverse sequence of oxide activity ($Al_2O_3 > TiO_2$) is observed, however, lower γ_S^D is obtained for SiO_2, which is close to that calculated using the equations of the Lifshitz theory.

The Table 3 shows also γ_S^D determined from data of inverse gas chromatography at finite concentrations at 403 K (Bogillo et al., 1996). As in previous case, γ_S^D

for SiO_2 is lower than for other oxides and for Al_2O_3 γ_S^D is higher than for TiO_2. If for SA_{30}, γ_S^D is between γ_S^D of individual SiO_2 and Al_2O_3, then γ_S^D for ST_{20} is significantly higher than that obtained for individual Si and Ti oxides. For the same oxide, the highest constant C of the BET equation (263) is observed (Table 1) compared with other oxides (93÷165) and, accordingly, the highest isosteric heat of adsorption, ΔQ_A (9.2 kJ mole^{-1}) in compared with the rest oxides (8.5÷8.9 kJ mole^{-1}).

The comparison of γ_S^D and γ^{S0} values for various silicas (Bilinski et al., 1999; Pokrovskiy et al., 1999) shows that these values depend on the method used, the temperature of preliminary sample preparation, the nature of the adsorbed substance, the adsorption temperature, and γ_S^D varies from 28.6 to 71 mJ m^{-2} (Bilinski et al., 1999), which coincides with $\gamma_{S\,(IGC)}^D$ and γ^{S0} values from the Table 3. Even greater variations are observed for γ_S^p (11.9÷160 mJ m^{-2}), which is associated with a significant influence of the choice of a polar adsorbed substance for determining this parameter (Bilinski et al., 1999). Similar significant variations in $\gamma_{S\,(IGC)}^D$ and γ^{S0} were also noted for other oxides, minerals, carbon and solid organic materials (Pokrovskiy et al., 1999). Slight variations of γ^{S0} for the studied oxides, in contrast to the calculated and experimental γ_S^D and the dependencies shown in Fig. 4, *c*, *d* suggest that the main contribution to γ^{S0} is made by its dispersive component.

The obtained parameters for the metal oxides allow evaluating the adsorption activity of their surface with respect to other trace gases in the Antarctic atmosphere. For these parameters it is necessary to calculate the partition coefficients of these gases between particles and the atmosphere, K_{SA}, and the kinetics of their removal from the atmosphere (Bogillo et al., 2008). The K_{SA} value for the adsorbed substance/material surface pair can be calculated by knowing the specific surface area of the material, its free surface energy, or the Hamaker' constant, as well as the γ^{LV} value (Bogillo et al., 1998; Pokrovskiy et al., 1999), or the critical temperature and critical pressure of the adsorbed substance (Mauer et al., 2001).

CONCLUSIONS

Using the volumetric method, low-temperature nitrogen adsorption isotherms on the surface of 12 fumed individual and mixed oxides of Si, Ti, and Al, as components of mineral aerosols in the Antarctic atmosphere, were measured. The aim of the work was to determine the effect of the origin and concentration of X, C_X in oxides of the X/SiO_2 type (X = Al_2O_3, TiO_2, Al_2O_3/TiO_2) on the structural and energetic characteristics of their surface.

Using the BET theory, the specific surface areas of the oxides, S_{BET}, were calculated. The relationship between C_X and S_{BET} for mixed oxides does not exist. Since the synthesis of oxides is carried out by hydrolysis of metal chlorides MCl_n (M = Si, Ti, and Al) in an oxygen/hydrogen flame at T > 1300 K, variations in T and the concentrations of O_2, H_2, and MCl_n, as well as the degree of crystallinity, probably significantly affect structural characteristics of primary particles and aggregates formed from them.

Using the regularization method, the surface distributions of the oxides on the N_2 adsorption energies were computed. It was found that their surface is characterized by a high degree of heterogeneity, manifested in the presence of several peaks in the distribution curves and their significant width. Since the upper limits of the distributions significantly exceed the heat of vaporization of N_2, this may be due to the significant contribution of the electrostatic interaction between the quadrupole molecule N_2 and dipoles of surface OH groups and ions in the overall adsorption energy.

Since the BET isotherm describes adsorption only in a limited narrow pressure range, the Zeta Adsorption Isotherm (ZAI) derived in the approximation of adsorbed vapor as a set of molecular clusters was used for its full range. ZAI describes isotherms well, and the specific surface areas of oxides, A_s, the maximum number of molecules in adsorbed clusters, the thickness of an adsorbed liquid film, and the free surface energies of oxides in the absence of adsorption, γ^{S0}, are calculated using the ZAI equations.

The A_s correlates well with S_{BET} and account for 77.5% of one, which may be due to the contribution

of the orthogonal orientation of N_2 molecules in clusters (ZAI), in contrast to their parallel orientation in the BET theory.

It was shown that γ^{S0} increase with rise of average adsorption energies of N_2. There is no dependence between γ^{S0} and C_X (taking into account γ^{S0} for X) for mixed oxides, which may be due to a higher content of SiO_2 in the shell of their particles, while Al_2O_3 and TiO_2 form mainly their core.

The γ^{S0} value of individual oxides increases with rise of their permittivity and refractive index. The γ^{S0} is in the range of dispersive components of the free surface energy determined by other experimental methods and calculated according to the Lifshitz theory.

These parameters for oxides make it possible to estimate the adsorption activity of their surface in relation to other trace gases in the Antarctic atmosphere, which is necessary to evaluate their partition coefficients between particles and the atmosphere and their removal kinetics.

Acknowledgements. Adsorption measurements were performed at the Adsorption and Chromatography Laboratory (Head is Prof. M. Jaroniec) of the Chemistry Department, Kent State University, Ohio, USA with financial support from the US National Science Foundation (COBASE program).

REFERENCES

1. Al-Abadleh, H. A., Grassian, V. H. 2003. Oxide surfaces as environmental interfaces. *Surface Science Reports*, 52. 63–161.
2. Artaxo, P., Rabello, M. L. C. 1992. Trace elements and individual particle analysis of atmospheric aerosols from the Antarctic Peninsula. *Tellus B.*, 44. 318—334.
3. Asmi, E., Neitola, K., Teinilä, K., Rodriguez, E., Virkkula, A., Backman, J., et al. 2018. Primary sources control the variability of aerosol optical properties in the Antarctic Peninsula. *Tellus B.*, 70:1414571. doi:10.1080/16000889.2017.1414571.
4. Atkins, C. B., Dunbar, G. B. 2009. Aeolian sediment flux from sea ice into southern McMurdo sound, Antarctica. *Global Planetary Change*, 69. 133—141.
5. Ayling, B. F., McGowan, H. A. 2006. Niveo-eolian sediment deposits in coastal South Victoria Land, Antarctica: indicators of regional variability in weather and climate. *Arctic, Antarctic and Alpine Research*, 38. 313—324.
6. Basile, I., Grousset, F. E., Revel, M., Petit, J. R., Biscaye, P. E., Barkov, N. I. 1997. Patagonian origin of glacial dust deposited in East Antarctica (Vostok and Dome C) during glacial stages 2, 4 and 6. *Earth Planet Science Letters*, 146. 573—589.
7. Bergstrom, L. 1997. Hamaker Constants of Inorganic Materials. *Advances in Colloid and Interface Science*, 70. 125—169.
8. Bilinski, B.. Holysz, L. 1999. Some Theoretical and Experimental Limitations in the Determination of Surface Free Energy of Siliceous Solids. *Powder Technology*, 102. 120—126.
9. Bogillo, V. I., Shkilev, V. P., Voelkel A. 1996. Chemical Heterogeneity of Metal Oxides Surface as Studied by Inverse Gas Chromatography at Finite Concentrations. *Adsorption Science and Technology*, 14(3). 189—198.
10. Bogillo, V. I., Shkilev, V. P., Voelkel, A. 1998. Determination of Surface Free Energy Components for Heterogeneous Solids by Means of Inverse Gas Chromatography at Finite Concentrations. *Journal of Materials Chemistry*, 8(9). 1953—1961.
11. Bogillo, V. I., Shkilev, V. P. 1999. Evaluation of Desorption Energy Distributions from TPD Spectra on the Heterogeneous Solid Surfaces. *Journal of Thermal Analysis and Calorimetry*, 55(2). 483—492.
12. Bogillo, V. I., Bazylevska, M. S. 2008. Partitioning and Exchange of Organochlorine Contaminants between Abiotic Compartments in Antarctica. In Mehmetli E. et al (eds). *The Fate of Persistent Organic Pollutants in the Environment,* Dordrecht: Springer. 333—351.
13. Bory, A., Wolff, E., Mulvaney, R., Jagoutz, E., Wegner, A., Ruth, U., et al. 2010. Multiple sources supply eolian mineral dust to the Atlantic sector of coastal Antarctica: evidence from recent snow layers at the top of Berkner Island ice sheet. *Earth Planet Science. Letters*, 291. 138—148.
14. Brunauer, S. Emmett, P. H., Teller, E. 1938. Adsorption of Gases in Multimolecular Layers. *Journal of American Chemical Society*, 60. 309—319.
15. Budhavant, K., Safi, P. D., Rao, P. S. P. 2015. Sources and elemental composition of summer aerosols in the Larsemann Hills (Antarctica). *Environmental Science and Pollution Research*, 22. 2041—2050.
16. Bullard, J. E., Baddock, M., Bradwell, T., Crusius, J., Darlington, E., Gaiero, D., et al. 2016. High-latitude dust in the Earth system. *Review of Geophysics*, 54. 447—485.
17. Chaubey, J. P., Moorthy, K. K., Babu, S. S., Nair, V. S. 2011. The optical and physical properties of atmospheric aerosols over the Indian Antarctic stations during southern hemispheric summer of the international Polar Year 2007–2008. *Annals of Geophysics*, 29. 109—121.
18. Chewings, J. M., Atkins, C., Dunbar, G., Golledge, N. R. 2014. Aeolian sediment transport and deposition in a

modern high-latitude glacial marine environment. *Sedimentology*, 61. 1535—1557.
19. Delmonte, B., Paleari, C. I., Andò, S., Garzanti, E., Andersson, P. S., Petit, J. R., et al. 2017. Causes of dust size variability in central East Antarctica (Dome B): atmospheric transport from expanded South American sources during marine isotope stage 2. *Quaternary Science Review*, 168. 55—68.
20. Dupart, Y., King, S. M., Nekat, B., Nowak, A., Wiedensohler, A., Herrmann, H., David, G., Thomas, B., Miffre, A., Rairoux, P., D'Anna, B., George, C. 2012. Mineral Dust Photochemistry Induces Nucleation Events in the Presence of SO_2. *Proceedings of National Academy of Sciences of USA*, 109(51). 20842—20847.
21. Dzyaloshinskii, I.E., Lifshitz, E.M., Pitaevskii, L.P. 1961. The General Theory of Van der Waals Forces. *Advances in Physics*, 10. 165—209.
22. Ghasemi, H., Ward, C. A. 2009. Determination of the Surface Tension of Solids in the Absence of Adsorption. *Journal of Physical Chemistry*, 113. 12632—12634.
23. Gregg, S. J., Sing, K. S. V. 1982. *Adsorption. Surface Area and Porosity*, London. New York: Academic Press Inc.
24. Gun'ko, V. M., Blitz, J. P., Gude, K., Zarko, V. I., Goncharuk, E. V., Nychiporuk, Y. M. Leboda, R., Skubiszewska-Zieba, J., Osovskii, V. D., Ptushinskii, Y. G., Mishchuk, O. A., Pakhovchishin, S. V., Gorbik, P. P. 2007. Surface Structure and Properties of Mixed Fumed Oxides. *Journal of Colloid and Interface Science*, 314(1). 119—130.
25. Israelachvili, J.N. 1992. Adhesion Forces between Surfaces in Liquids and Condensable Vapours. *Surface Science Reports*, (14). 109—159.
26. Kavan, J., Ondruch, J., Nývlt, D., Hrbá¡cek, F., Carrivick, J. L., Láska, K. 2017. Seasonal hydrological and suspended sediment transport dynamics in proglacial streams, James Ross Island, Antarctica. *Geography Annals*, 99. 38—55.
27. Lancaster, N. 2002. Flux of eolian sediment in the McMurdo Dry Valleys, Antarctica: a preliminary assessment. *Arctic, Antarctic and Alpine Research*, 34. 318—323.
28. Mauer, S., Mersmann, A., Peukert, W. 2001. Henry Coefficients of Adsorption Predicted from Solid Hamaker Constants. *Chemical Engineering Science*, 56. 3443—3453.
29. Mazzera, D. M., Lowenthal, D., Chow, J. C., Watson, J. G., Grubisic, V. 2001. PM_{10} measurements at McMurdo station, Antarctica. *Atmospheric Environment*, 35. 1891—1902.
30. McConnell, J. R., Aristarain, A. J., Banta, J. R., Edwards, P. R., Simoes, J. C. 2007. 20th-Century doubling in dust archived in an Antarctic peninsula ice core parallels climate change and desertification in South America. *Proceedings of National Academy of Sciences of U. S. A.*, 104. 5743—5748.
31. Medout-Marere, V. 2000. A Simple Experimental Way of Measuring the Hamaker Constant A_{11} of Divided Solids by Immersion Calorimetry in Apolar Liquids. *Journal of Colloid and Interface Science*, 228. 434—437.
32. Ne, P. D., Bertler, N. A. N. 2015. Trajectory modeling of modern dust transport to the Southern Ocean and Antarctica. *Journal of Geophysics Research Atmosphere*, 120. 9303—9322.
33. Pereira, K. C. D., Evangelista, H., Pereira, E. B., Simoes, J. C., Johnson, E., Melo, L. R. 2004. Transport of crustal microparticles from chilean Patagonia to the Antarctic peninsula by SEM-EDS analysis. *Tellus B.*, 56. 262—275.
34. Pokrovskiy, V. A., Bogillo, V. I., Dabrowski, A. 1999. Adsorption and Chemisorption of Organic Pollutants on the Solid Aerosols Surface. In. Dabrowski A. (ed). *Adsorption and its Application in Industry and Environmental Protection*. Amsterdam: Elsevier. 571—634.
35. Prausnitz, J. M. 1966. Surface Tension of Simple Liquids. *Transactions of Faraday Society*, 62. 1097—1104.
36. Pyziy, A. M., Volcov, V. B., Poznayeva, O. A., Bogillo, V. I. Shkilev, V. P. 1997. Comparison of Various Numerical Procedures for Analysis of Structural Heterogeneity. *Langmuir*, 13(5). 1303—1306.
37. Seinfeld, J.H., Pandis, S. N. 2006. *Atmospheric Chemistry and Physics: From Air Pollution to Climate Change*, London, New York: John Wiley & Sons, Inc.
38. Truzzi, C., Lambertucci, L., Illuminati, S., Annibaldi, A., Scarponi, G. 2005. Direct gravimetric measurements of the mass of the Antarctic aerosol collected by high volume sampler: PM_{10} summer seasonal variation at Terra Nova Bay. *Annals of Chemistry*, 95. 867—876.
39. Weller, R., Wöltjen, J., Piel C., Resenberg, R., Wagenbach, D., König-Langlo, G., et al. 2008. Seasonal variability of crustal and marine trace elements in the aerosol at Neumayer station, Antarctica. *Tellus B.*, 60. 742—752.
40. Zandavi, S. H. Ward, C. A. 2014. Clusters in the Adsorbates of Vapours and Gases: Zeta Isotherm Approach. *Physical Chemistry and Chemical Physics*, 16. 10979—10989.

М. С. Базилевська, В. Й. Богилло*

Інститут геологічних наук, Національна академія наук України,
вул. Олеся Гончара, 55Б, м. Київ, 01054, Україна

* Автор для кореспонденції: bazilevskaya1955@gmail.com

АДСОРБЦІЙНІ ВЛАСТИВОСТІ ПІРОГЕННИХ ІНДИВІДУАЛЬНИХ І ЗМІШАНИХ ОКСИДІВ SI, TI ТА AL ЯК МОДЕЛЕЙ МІНЕРАЛЬНИХ АЕРОЗОЛІВ В АТМОСФЕРІ АНТАРКТИКИ

РЕФЕРАТ. **Метою** роботи було визначення впливу природи та вмісту X, C_X в оксидах X/SiO_2 ($X = Al_2O_3$, TiO_2, Al_2O_3/TiO_2) на характеристики їх поверхні. **Методом** волюметрії виміряні низькотемпературні ізотерми адсорбції азоту на поверхні 12 індивідуальних і змішаних пірогених оксидів Si, Ti та Al, як компонентів мінеральних аерозолів в атмосфері Антарктики. Згідно теорії БЕТ розраховано питомі площі поверхні оксидів, S_{BET}. Залежності між C_X і S_{BET} для змішаних оксидів не виявлено, що пов'язано з впливом температури реакції гідролізу MCl_n (M = Si, Ti та Al) у кисень/водневому полум'ї та відношень концентрацій O_2, H_2 і MCl_n на структурні характеристики первинних частинок та агрегатів. **Методом** регуляризації розраховано розподіли поверхні оксидів за енергіями адсорбції N_2 та показано, що вона характеризується високою мірою енергетичної неоднорідності. Для опису адсорбції N_2 у повному діапазоні його тисків застосовано Зета – ізотерму адсорбції (ZAI), яку отримано в наближенні адсорбованого пару, як набору кластерів молекул. За рівняннями ZAI розраховано питомі площі поверхні оксидів, A_s, максимальні кількості молекул в адсорбованих кластерах, товщини адсорбованої рідкої плівки та вільні поверхневі енергії оксидів за відсутності адсорбції, γ^{S0}. A_s гарно корелює з S_{BET} та складає 77,5% від неї. Величина γ^{S0} зростає при збільшенні середньої енергії адсорбції N_2. Залежності між γ^{S0} та C_X (з урахуванням γ^{S0} для X) для змішаних оксидів не виявлено. Для SiO_2, Al_2O_3 і TiO_2 γ^{S0} зростає при збільшенні діелектричної проникності оксидів та показника заломлення і знаходяться в діапазоні їх дисперсійних компонент вільної поверхневої енергії, які визначено іншими експериментальними методами та розраховано згідно теорії Ліфшиця. Знайдені параметри для оксидів дозволяють оцінити активність їх поверхонь по відношенню до домішок в атмосфері Антарктики, що необхідно для розрахунку їх коефіцієнтів розподілу між частинками та атмосферою і кінетики їх видалення.

Ключові слова: мінеральні аерозолі, атмосфера Антарктики, пірогенні індивідуальні та змішані оксиди Si, Ti та Al, адсорбція азоту.